Radiology

ORIGINAL RESEARCH • HEAD AND NECK IMAGING

Deep Learning for Head and Neck CT Angiography: Stenosis and Plaque Classification

Fan Fu, PhD • Yi Shan, PhD • Guang Yang, MD • Chao Zheng, MD • Miao Zhang, PhD • Dongdong Rong, PhD • Ximing Wang, PhD • Jie Lu, PhD

From the Department of Radiology and Nuclear Medicine, Xuanwu Hospital, Capital Medical University, No. 45 Changchun St, Xicheng District, Beijing 100053, China (F.F., Y.S., M.Z., D.R., J.L.); Beijing Key Laboratory of Magnetic Resonance Imaging and Brain Informatics, Beijing, China (F.F., Y.S., M.Z., D.R., J.L.); Department of Nuclear Medicine, Ruijin Hospital, Shanghai Jiaotong University, Shanghai, China (F.F.); Shukun (Beijing) Technology Co, Beijing, China (G.Y., C.Z.); and Department of Radiology, Shandong Provincial Hospital, Jinan, China (X.W.). Received April 22, 2022; revision requested June 22; revision received December 2; accepted January 24, 2023. **Address correspondence to** J.L. (email: *imaginglu@hotmail.com*).

Supported by the Beijing Natural Science Foundation (grant Z190014), National Natural Science Foundation of China (grant 82130058), and Beijing Municipal Science and Technology Projects (grant Z201100005620009).

Conflicts of interest are listed at the end of this article.

Radiology 2023; 000:e220996 • https://doi.org/10.1148/radiol.220996 • Content codes: HN CT

Background: Studies have rarely investigated stenosis detection from head and neck CT angiography scans because accurate interpretation is time consuming and labor intensive.

Purpose: To develop an automated convolutional neural network–based method for accurate stenosis detection and plaque classification in head and neck CT angiography images and compare its performance with that of radiologists.

Materials and Methods: A deep learning (DL) algorithm was constructed and trained with use of head and neck CT angiography images that were collected retrospectively from four tertiary hospitals between March 2020 and July 2021. CT scans were partitioned into training, validation, and independent test sets at a ratio of 7:2:1. An independent test set of CT angiography scans was collected prospectively between October 2021 and December 2021 in one of the four tertiary centers. Stenosis grade categories were as follows: mild stenosis (<50%), moderate stenosis (50%–69%), severe stenosis (70%–99%), and occlusion (100%). The stenosis diagnosis and plaque classification of the algorithm were compared with the ground truth of consensus by two radiologists (with more than 10 years of experience). The performance of the models was analyzed in terms of accuracy, sensitivity, specificity, and areas under the receiver operating characteristic curve.

Results: There were 3266 patients (mean age ± SD, 62 years ± 12; 2096 men) evaluated. The consistency between radiologists and the DL-assisted algorithm on plaque classification was 85.6% (320 of 374 cases [95% CI: 83.2, 88.6]) on a per-vessel basis. Moreover, the artificial intelligence model assisted in visual assessment, such as increasing confidence in the degree of stenosis. This reduced the time needed for diagnosis and report writing of radiologists from 28.8 minutes ± 5.6 to 12.4 minutes ± 2.0 ($P < .001$).

Conclusion: A deep learning algorithm for head and neck CT angiography interpretation accurately determined vessel stenosis and plaque classification and had equivalent diagnostic performance when compared with experienced radiologists.

Supplemental material is available for this article.

Globally, cerebrovascular disease remains the leading cause of severe disability and mortality (1). Atherosclerosis is frequently associated with cerebrovascular events. The degree of artery stenosis is considered one of the parameters for therapeutic options (2,3). Head and neck CT angiography has emerged as a front-line approach to assess the atherosclerotic process and gained worldwide clinical acceptance (4). However, the interpretation of CT angiography still requires detailed evaluation of all cervical vascular structures, which is a time-intensive process (5). Moreover, there is interobserver variability in the visual assessment of stenosis degree and plaque composition (6,7).

Deep learning (DL)–based approaches have drawn increasing interest due to the incremental data-driven iteration and generalization abilities from large data volumes (8,9). In radiology, DL has been applied in several assisting roles, such as generation of contrast-enhanced T1-weighted scans from precontrast MRI scans in patients with breast cancer (10), quantification of calcium score with coronary CT angiography (11), automated detection of cerebral aneurysms with CT angiography (12), prioritization in radiologic workflow and reduction of time to diagnosis of intracranial hemorrhage with nonenhanced CT images (13), and detection of pulmonary nodules with chest CT images (14). Computer-aided investigation of acute neurologic disorders in neuroimaging may play a role in the triage of radiologic workflow, resulting in shorter time to diagnosis and improved management outcomes (15).

In past years, various DL models have shown potential for coronary artery stenosis detection and plaque quantification (16–19). Convolutional neural networks have also been used for segmentation and automatic stenosis quantification with use of CT angiography images (20,21). Also, several studies have applied convolutional neural network models to achieve plaque classification and quantification in carotid artery atherosclerosis (4,22,23). However, studies have rarely investigated stenosis detection from head and neck CT angiography scans due to the wide range

Abbreviations

AI = artificial intelligence, DL = deep learning

Summary

In a multicenter study, a deep learning algorithm for evaluation of head and neck CT angiography had equivalent diagnostic performance for arterial stenosis and plaque classification compared with experienced radiologists.

Key Results

- In a multicenter study, a deep learning algorithm trained with use of the head and neck CT angiography scans of 3266 patients had 90% and 81% accuracy in an independent test set of 327 scans for stenosis diagnosis and plaque classification, respectively (all indicators: area under the receiver operating characteristic curve > 0.85).
- There was high agreement between the algorithm and ground truth of consensus by two radiologists on stenosis detection ($\kappa = 0.84$), plaque classification ($\kappa = 0.78$), and diameter stenosis ($R = 0.87$, $P < .001$).
- The algorithm reduced the diagnosis and report writing time of radiologists from 28.8 minutes ± 5.6 to 12.4 minutes ± 2.0 ($P < .001$).

from the aorta to skull and the tortuous and branched arterial brain vessels.

The purpose of this study was to develop an automated convolutional neural network–based method for accurate stenosis detection and plaque classification with head and neck CT angiography images and compare its performance with that of radiologists.

Materials and Methods

The study was approved by the institutional review board of the University Medical Center. Written informed consent for all patients were obtained in Capital Medical University Xuanwu Hospital for the 142 prospectively collected images.

Data Preparation

We retrospectively collected the images from four tertiary hospitals between March 2020 and July 2021. All submissions and previous reports were not overlapped with the current work. Inclusion criteria included raw contrast-enhanced head and neck CT angiography images with suspected cerebrovascular disease decided by clinicians (based on age, sex, risk factors, clinical symptoms such as motor and/or sensory issues, alalia, stupor and/or coma, limb weakness, numb, headache, dizziness and/or vertigo, etc). Images with severe artifacts, lack of image data, and poor imaging quality were excluded. The patient CT angiography images were in Digital Imaging and Communications in Medicine, or DICOM, format, and the scans were acquired from three different CT scanners. The imaging protocol included standard head and neck CT angiography with variable imaging parameters (Table S1).

For the independent test set, 142 additional head and neck CT angiography images were prospectively selected between October 2021 and December 2021 to assess the diagnostic performance of the model. The overall workflow diagram of the experimental design is shown in Figure 1.

Radiologist Annotations

All images were anonymized. To ensure the accuracy of the annotation, we adopted a hierarchical labeling method for all the scans in the database. Data were labeled on the reconstructed images and the original axial images with ITK-SNAP software (version 3.6, University of Utah) (24) (Fig S1). The lumen labeled at 36 different angles with straightened rendering images and the two-dimensional segmentation of the vessel was annotated without any plaque and branching vessels. Based on the extracted plaque candidate area on original images, artificial intelligence (AI) annotated the plaques and plaque type (calcified plaque, noncalcified plaque, mixed plaque). Then, 10 technologists (two of whom were authors F.F. and Y.S., with 2–4 years of clinical experience) independently labeled the vessel lumen and plaque with masks. After that, two radiologists (M.Z. and D.R., with 12 and 14 years of experience in neuroimaging, respectively) double-checked the preliminary labeling results and relabeled cases. When disagreements occurred, an arbitrator (J.L., with 20 years of experience in neuroimaging) made the final decision.

Model Development

The core design of the CerebralDoc system was a DL model. The model was divided into two parts: a two-dimensional ResU-Net combined multiangle vessel stenosis auto-detection model and a three-dimensional ResU-Net combined multifeature sequence callback model (Fig 2). Accurate extracting centerline plays an important role in stenosis detection. Thus, a weighted skeleton method (25) combined with the topology of prior knowledge was used to obtain the most accurate center trend line. The CT value of the area near the blood vessel boundary was used as a weight reference to optimize the precise position of the center point.

Then, two-dimensional ResU-Net was applied to the reconstructed images, with 36 different angles responsible for the segmentation of vessel lumen. Straightened rendering images were adopted in this task to precisely visualize and annotate the vessel lumen with the attention model (Fig S2). Three-dimensional ResU-Net was applied to original axial images responsible for segmentation of plaque. The multifeature sequence callback model was designed to remove false-positive findings (Fig S3). The online software is accessible at: *http://test.platform.shukun.net/login*. To log in, use username: test and password: 123456. Code is available at: *https://bitbucket.org/zchao_sk/cerebral/src/master/*.

Auto Image Layout and Structured Reports

All the head and neck CT angiography images were processed for vessel segmentation and reconstruction by an automatic imaging reconstruction system that had been reported before (26). Multiple planners reformat, curve planner reformat, maximum intensity projection, and volume rendering images of all vessels were reconstructed. The four output images were placed in the first row of the film image produced by the junior AI system and could be verified and overwritten by technologists. After the technologist's verification, the reconstructed images are exported to the diagnostic system.

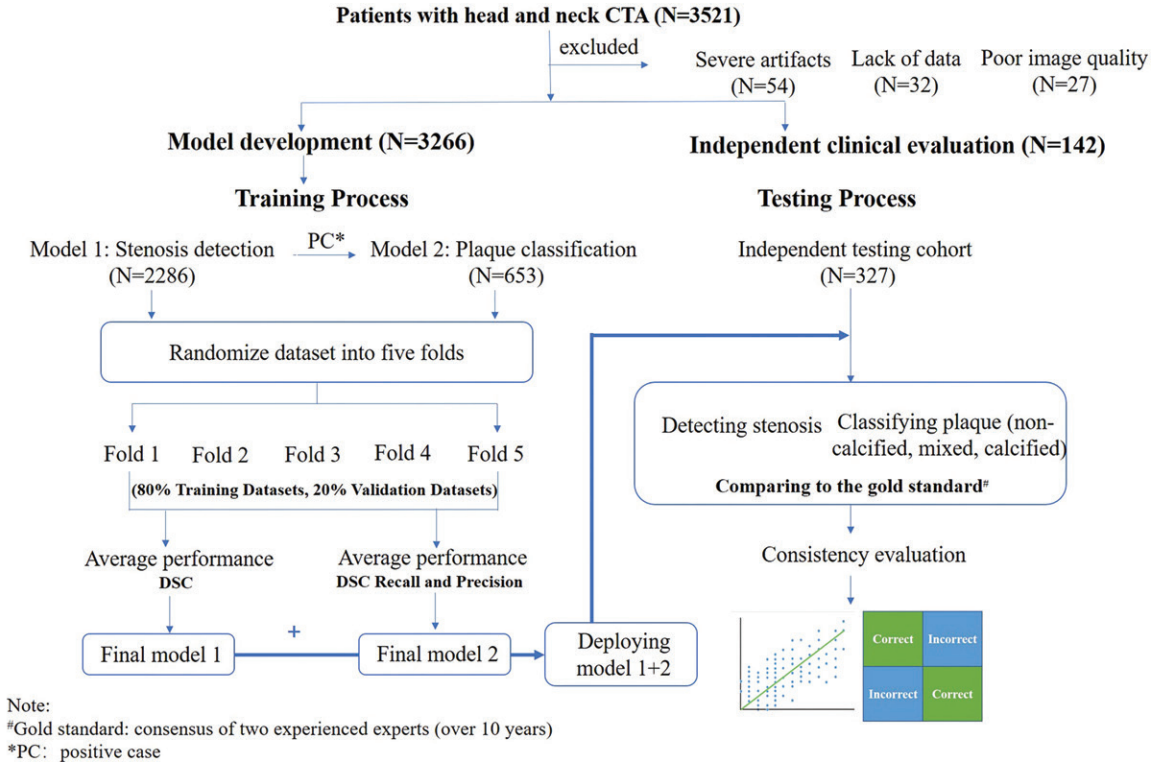

Figure 1: Experimental setting diagram shows the algorithm approach at achieving stenosis detection and plaque classification. The training process was divided into two parts with two overlapping training sets. Two models derived from ResU-Net were assessed for performance evaluation by the average value of fivefold index. Then, the better performance of the model was obtained after rounds of training iterations. The final two models were deployed to an independent test set with 327 patients to manifest the credibility of deep learning–assisted algorithm by accuracy and consistency analysis. CTA = CT angiography, DSC = Dice similarity score.

The diagnostic system first captures and places the most significant stenosis (≥50%) in the left row of the film image page and achieves productivity by enabling traceability. The narrowing area can also be verified and overwritten by radiologists. The output of the adaptive layout tool included the location and degree of stenosis, plaque composition, and a final structured report (Fig S4).

Performance Metrics

Model effectiveness.—Model performance was measured by lumen and calcification segmentation Dice similarity score, calcification recall, and calcification precision, which were evaluated by all plaques and lumen vessels, so the segmentation of plaques was per plaque, while the segmentation of the lumen vessels was per vessel.

Clinical evaluation.—Two radiologists (M.Z. and D.R.) performed the assessment of the head and neck CT angiography images blinded to the clinical indication, radiologic reports, and other imaging examinations. After reading randomly and solving any disagreement by discussion, they came to a consensus representing the ground truth for the study. Stenosis grade categories were as follows: mild stenosis (<50%), moderate stenosis (50%–69%), severe stenosis (70%–99%), and occlusion (100%). Lumen diameter with 50% stenosis or more was considered clinically significant and quantitative measurements were made in maximal stenosis diameter up to a luminal diameter limit of at least 1.5 mm. The diagnostic performance was compared between AI and visual inspection on per-patient and per-vessel level, respectively. Moreover, a plaque was characterized as noncalcified plaque (including fibrous, fibro-fatty, and necrotic core), mixed plaque, and calcified plaque. The mixed plaque is the mixture of noncalcified component and calcification. Calcified plaque based upon Hounsfield unit densities of greater than 350 HU (18). Of the moderate and severe stenosis, the threshold stenosis was 45%–55% and 70%–80%, respectively.

There were 142 CT angiograms assigned to each of the two radiologists (F.F. and Y.S.) for random interpretation either with or without aid of the algorithm. Following a 1-month washout period, the same selected sample was randomly interpreted again by the same corresponding radiologist with or without aid of the algorithm (if the first read was with algorithm aid, then the second read was without algorithm aid). The average diagnosis and report writing time, overall time (including reconstruction, diagnosis, and report writing), and diagnostic efficiency (defined as the detected numbers of stenosis per unit time) of AI and radiologists were recorded.

Statistical Analysis

All the analyses were conducted with use of SPSS software version 23.0 (IBM). Spearman correlation coefficient was used to assess correlation between AI and radiologists in maximum percentage stenosis. Bland-Altman plots were used to evaluate the consensus between AI and radiologists for determined maxi-

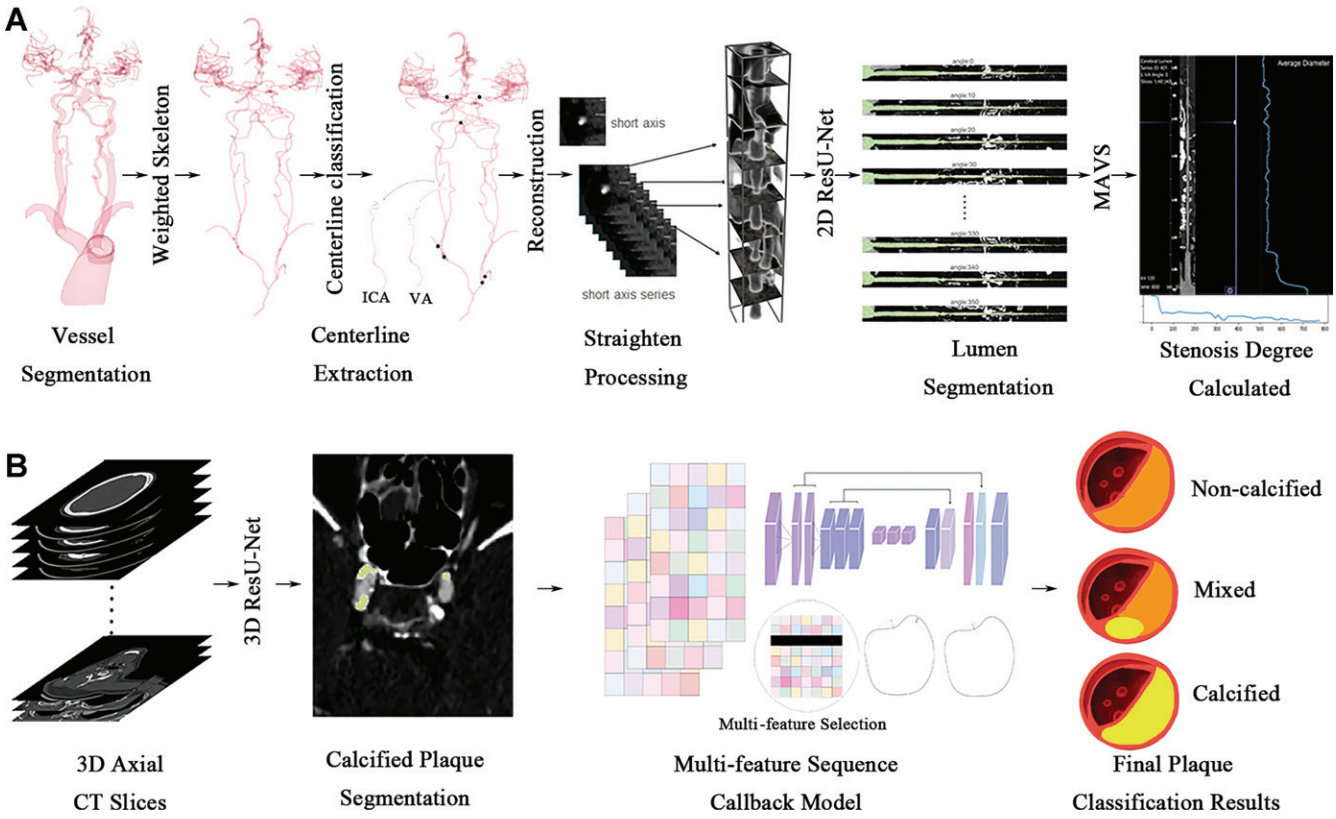

Figure 2: Diagnosis framework shows the artificial intelligence software pipeline. **(A)** Based on the reconstruction image proposed before, a weighted skeleton method was used to extract the centerline. The formula was (M1−Vct)/(M1−M0). M1 is the vessel mean value, M0 is the background mean value, and Vct is the CT value of the current voxel. We also used the specific topology as prior knowledge to make the centerline direction more accurate. Then, two-dimensional (2D) ResU-Net was applied to the straightened rendering images for vessel lumen segmentation. Additionally, a multiangle vessel stenosis auto-detection model was applied to calculate the stenosis degree for each point of the vessel centerline. Straightened rendering images rather than three-dimensional (3D) vessel segmentation images were used in this pipeline to avoid useless information, such as vessel branches that cause inaccurate stenosis calculation. Also, the network can work with light input data instead of large original data. **(B)** Three-dimensional ResU-Net was applied to original axial images for the segmentation of plaque. The input to the network was original three-dimensional volume data, which was split into 64 × 64 × 64. Then, the multifeature sequence callback model was used to reduce the false-positive rate caused by plaque segmentation. Finally, the probability of plaque type is output in a one-dimensional sequence. ICA = internal carotid artery, MAVS = multiangle vessel stenosis, VA = vertebral artery.

mal diameter stenosis. Weighted κ statistic was used to measure agreement between AI and radiologists. Diagnostic performance of AI was assessed through diagnostic accuracy, sensitivity, specificity, and positive and negative predictive values, as compared with the ground truth by radiologists. The diagnostic performances of AI and visual assessment for luminal stenosis were evaluated by the area under the receiver operating characteristic curves. Covariance test was used to compare the consumed time of AI and radiologists with the increase of diseased vessels. $P < .05$ were considered to indicate a statistically significant result. Statistical analysis was performed by two authors (F.F. and G.Y., with 8 years of experience in algorithm).

Results

Patient Characteristics

Of 3521 head and neck CT angiography scans, 113 (3.2%) CT angiography scans were excluded based on severe artifacts (n = 54), lack of image data (n = 32), and poor imaging quality (n = 27) (Fig 1). In total, after exclusions, 3266 consecutive patients (mean age ± SD, 62 years ± 12; 2096 men) who underwent head and neck CT angiography at three tertiary hospitals (from March 2020 to July 2021) were included for model development. In addition, 142 patients (mean age, 61 years ± 11; 79 men) prospectively underwent CT angiography for clinical evaluation (independent test set). The demographic data and baseline clinical variables for model development and clinical evaluation are depicted in Table 1.

Model Performance

During the training process, the Dice similarity scores for the calcification segmentation of plaque were 0.95 (95% CI: 0.92, 0.98) and 0.88 (95% CI: 0.85, 0.91), recall of 0.96 and 0.94, and calcification precision of 0.93 and 0.85 for the training and validation sets, respectively. The vessel lumen segmentation obtained Dice similarity scores of 0.96 (95% CI: 0.93, 0.97) and 0.95 (95% CI: 0.92, 0.97) for the training and validation sets. In the independent test set used to evaluate model performance, this model achieved an accuracy of stenosis diagnosis of 90% with 19 occluded arteries and all these arteries were detected by AI (Fig S5).

Diagnostic Performance of Stenosis in Patient-based Analysis

Among the 142 patients, 120 (85%) with significant stenosis were identified by radiologists, while 118 (83%) were identi-

Table 1: Demographic Data

Parameter	Model Development*	Clinical Evaluation†
Patients	3266 (2286/653/327)	142
M	2096 (1465/459/172)	79
F	1170 (821/194/155)	63
Age ± SD (y)‡	62 ± 12 (60 ± 10/63 ± 14/61 ± 12) [38–39]	61 ± 11 [42–81]
CVD prevalence§	85 (83/88/85)	85
Hypertension	1688 (1212/354/122)	94
Hyperlipidemia	1810 (1320/366/124)	108
Diabetes	975 (621/254/100)	43
Smoking	1083 (792/186/105)	75
Antiplatelet therapy	1011 (767/194/50)	34

Note.—Data are numbers of patients, unless otherwise noted. CVD = cerebrovascular disease.

* Data in parentheses are training/validation/independent test set.

† Data are independent test sets.

‡ Data in brackets are IQRs.

§ Data are percentages.

fied by AI (artifacts in six patients were mistaken as calcification artifacts, and artifacts in four patients were mistaken as failed reconstruction) (Fig 3). The weighted κ coefficient between the consensus of AI and radiologists in patient-based stenosis detection was 0.84 ± 0.02. Diagnostic performance of AI had good consistency with experienced radiologists.

The accuracy, sensitivity, specificity, positive predictive value, and negative predictive value of AI in at least 50% of stenosis was 93%, 95%, 83%, 97%, and 77%, respectively. Furthermore, in moderate (50%–69%) and severe stenosis (≥70%), the diagnostic performance of the AI model was shown in Table 2.

There was high agreement between the consensus of AI and radiologists in percent maximal stenosis (R = 0.80, P < .001). Bland-Altman plots depicted close mean differences between AI and radiologist consensus of 0.7% (95% CI: −0.6, 2.0) per patient (Fig 4).

Diagnostic Performance of Stenosis on Vessel-based Analysis

A total of 142 patients and 1846 vessels were included for analysis. The significant stenosis (≥50%) was depicted in 465 vessels (25.2%) by AI and 449 vessels (24.3%) by radiologists (Fig S6). A discordance of 54.4% was primarily seen in the threshold stenosis (Fig S7). The weighted κ coefficient between the consensus of AI and radiologists in vessel-based stenosis detection was 0.80 ± 0.03.

The accuracy, sensitivity, specificity, positive predictive value, and negative predictive value of AI in at least 50% stenosis was 94%, 90%, 95%, 86%, and 97%, respectively. Moreover, in moderate (50%–69%) and severe (≥70%) stenosis, the diagnostic performance of the AI model showed high agreement between the AI model and radiologist on diameter stenosis (R = 0.87, P < .001) (Table 2). Bland-Altman plots depicted close mean differences between the AI and radiologist consensus of 0.8% (95% CI: −0.6, 1.5) per vessel (Fig 4).

Plaque Classification Ability

In total, 465 nonnegligible plaques were detected in this study. The diagnostic accuracy of AI in identifying plaque classification is depicted in Table 3. The overall agreement index (κ) and accuracy were 0.78 ± 0.03 and 85.6% (95% CI: 80.1, 91.2), respectively. The accuracy of AI and radiologists in noncalcified plaque, mixed plaque, and calcified plaque was 80.7%, 81.3%, and 91.8%. The consistency was relatively better in identifying calcified plaque than noncalcified (P < .001).

Clinical Application Performance of DL-assisted Algorithm

The algorithm reduced the diagnosis and report writing time of radiologists from 28.8 minutes ± 5.6 to 12.4 minutes ± 2.0 (P < .001) (Fig 5A). Diagnostic efficiency was improved from 11% (95% CI: 10.2, 12.1) to 28% (95% CI: 26.5, 29.6) with use of the algorithm (P < .001) (Fig 5B). There was a significant difference between the AI and radiologist for diagnosing reporting time (F = 48.6, P < .001) and overall time (F = 59.3, P < .001) (Fig 5C) with the increase of diseased vessels. Moreover, in the description of stenosis, AI could provide quantitative numbers to radiologists (Fig 6).

The combined system reduced the overall time (including postprocessing, imaging interpretation, and complete junior diagnosis) from 45.2 minutes ± 4.3 to 14.2 minutes ± 1.4, facilitating clinical workflows (Fig S8).

Discussion

Interpreting head and neck CT angiography examination for clinical care is a time-consuming and labor-intensive process and requires expertise in cerebrovascular imaging. An artificial intelligence–based system that automatically processes head and neck CT angiography examinations, including the extraction of bone and vessels branch centerlines, as well as detection and localization of the atherosclerotic changes, could serve as a valuable tool to assist the clinicians. Thus, we aimed to develop an automated convolutional neural network–based method to provide accurate stenosis detection and plaque classification in head and neck CT angiography images. Moreover, the efficacy of the deep learning (DL) technique on image analysis was compared with experienced radiologists. Our results indicated that the DL algorithm could be trained to complete lumen and plaque segmentation automatically in a wide variety of enhanced CT angiography scans. There was high agreement between the algorithm and radiologists on stenosis detection (κ = 0.84), plaque classification (κ = 0.78), and diameter stenosis (R = 0.87, P < .001). Moreover, the algorithm reduced the diagnosis and report writing time of radiologists from 28.8 minutes ± 5.6 to 12.4 minutes ± 2.0 (P < .001).

Since 2011, convolutional neural networks have acquired many outstanding achievements in the segmentation, detection, and identification of regions within medical images (5,27,28). In our previous study, we developed a computational tool that could automatically extract entire vessels from head and neck scans and finish image reconstruction (26). Studies show the segmentation performance of convolutional neural networks is better than traditional methods (eg, region growth and some mixed traditional machine learning methods) (29,30). Prior studies (7,16,17) that used DL for stenosis quantification mostly did segmentation on

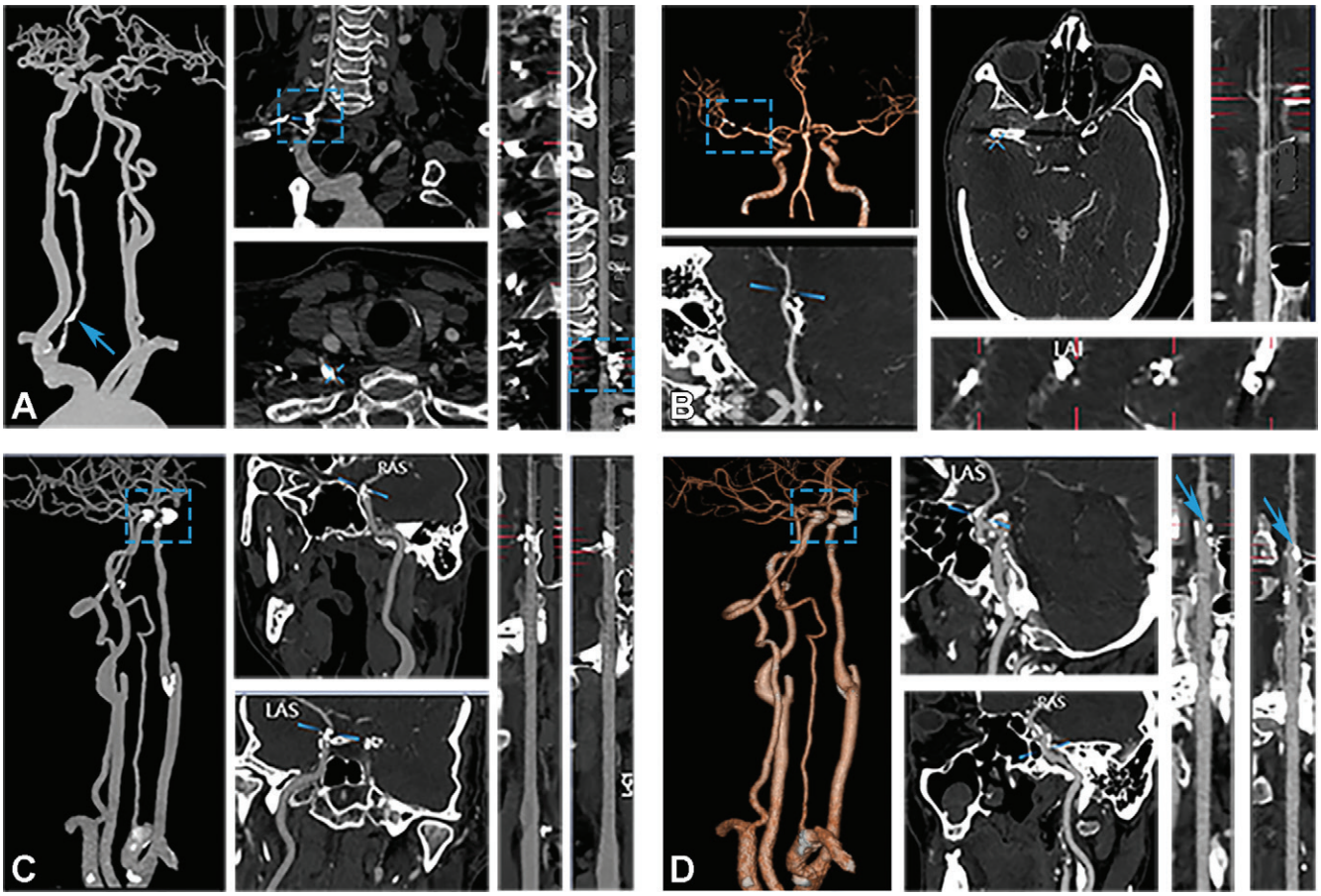

Figure 3: Multiple planners reformat, curve planner reformat, maximum intensity projection, and volume rendering images show examples of misdiagnoses by artificial intelligence (AI) (arrow and boxes). **(A)** Images show misidentification of artifacts as severe stenosis by AI. **(B)** Images show artifacts caused by intracranial aneurysm clipping mistaken as severe stenosis by AI (box). **(C, D)** Images show the wall calcification had obvious beam hardening artifacts that made the overestimation of stenosis degree by AI (arrows and boxes). LAS = left anterior superior, RAS = right anterior superior.

Table 2: Diagnostic Performance of CT Angiography Algorithm Compared with Radiologists

Threshold Classification	At Least 50% Stenosis		50%–69% Stenosis		At Least 70% Stenosis	
	Per Vessel	Per Patient	Per Vessel	Per Patient	Per Vessel	Per Patient
Accuracy	94 (1139/1847) [0.93, 0.95]	93 (133/144) [0.89, 0.97]	96 (1776/1847) [0.95, 0.97]	86 (122/142) [0.80, 0.92]	96 (1779/1847) [0.95, 0.97]	87 (124/142) [0.84, 0.90]
Sensitivity	90 (405/449) [0.87, 0.93]	95 (114/120) [0.89, 0.98]	92 (186/202) [0.87, 0.95]	95 (86/91) [0.87, 0.98]	83 (204/247) [0.77, 0.87]	91 (85/93) [0.83, 0.96]
Specificity	95 (1134/1398) [0.94, 0.96]	83 (20/24) [0.64, 0.93]	97 (1590/1645) [0.96, 0.97]	71 (36/51) [0.56, 0.82]	98 (1575/1600) [0.98, 0.99]	80 (39/49) [0.65, 0.89]
PPV	86 (405/469) [0.83, 0.89]	97 (114/118) [0.91, 0.99]	77 (186/241) [0.71, 0.82]	85 (86/101) [0.76, 0.91]	89 (204/229) [0.84, 0.93]	90 (85/95) [0.81, 0.95]
NPV	97 (1334/1378) [0.96, 0.98]	77 (20/26) [0.60, 0.92]	99 (1590/1606) [0.99, 1.00]	88 (36/47) [0.78, 0.98]	97 (1575/1618) [0.97, 0.99]	83 (39/47) [0.77, 0.87]
AUC*	0.93 [0.89, 0.95]	0.88 [0.79, 0.98]	0.94 [0.92, 0.97]	0.83 [0.75, 0.91]	0.91 [0.88, 0.93]	0.86 [0.78, 0.93]

Note.—Data are percentages, with numbers of patients in parentheses and 95% CIs in brackets. AUC = area under the receiver operating characteristic curve, NPV = negative predictive value, PPV = positive predictive value.

* Data are AUC values with 95% CIs in brackets.

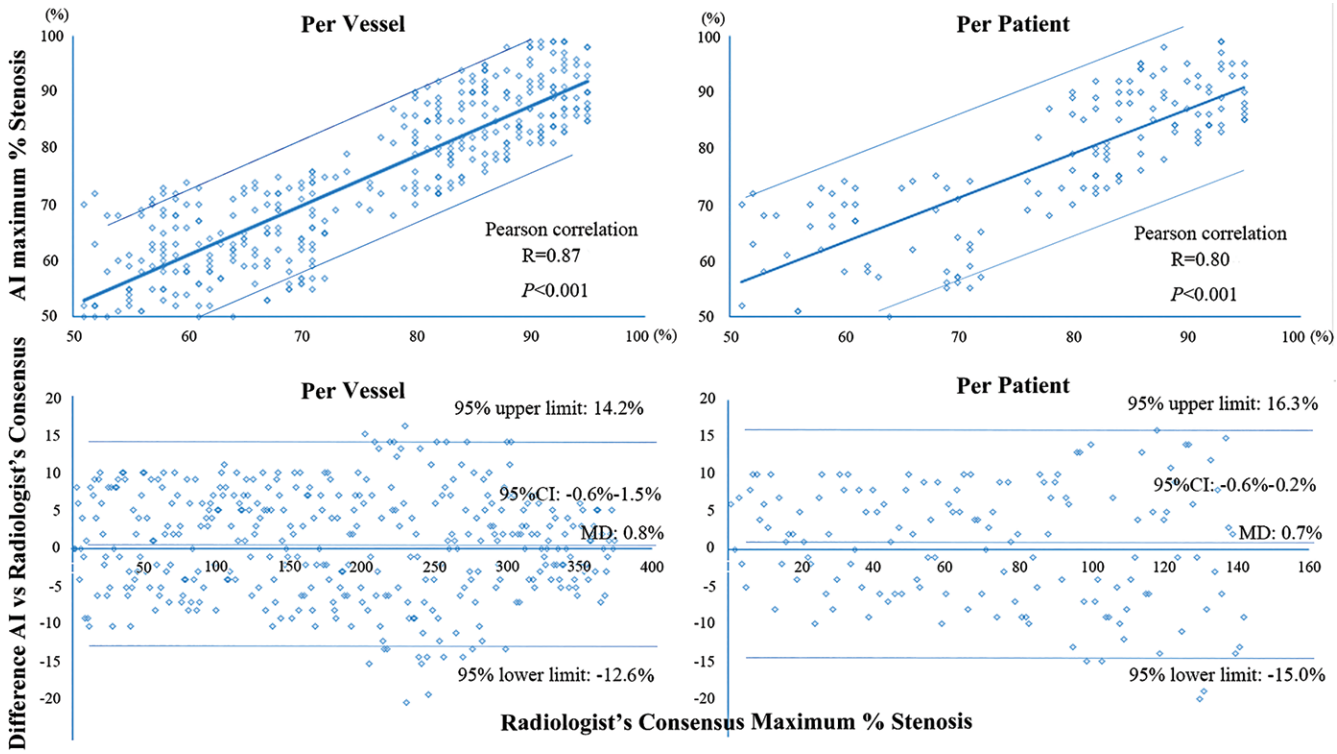

Figure 4: Linear regression and Bland-Altman plots show radiologist versus artificial intelligence (AI). Linear regression plots depict a close relationship between radiologist and AI diameter stenosis on both per-vessel and per-patient basis. Bland-Altman plots demonstrate good numeric agreement between radiologist and AI determined maximal diameter stenosis for per vessel and per patient. MD = mean difference.

Table 3: Diagnostic Accuracy and Agreement of Plaque Classification

Classification	Artificial Intelligence	Radiologists	Accuracy (%)
Noncalcified plaque	75	93	80.7
Calcified plaque	145	158	91.8
Mixed plaque	100	123	81.3
Total	320	374	85.6
Agreement index (κ)	0.78	$P < .001$	…

Note.—Data are numbers of artificial intelligence models and radiologists used, unless otherwise noted.

the original axial view or typical curve planner reformat view. However, the segmentation on axial view or single curve planner reformat view has some limitations, such as missing the complete vessel information. In our study, the vessel segmentation was performed on straightened rendering view, providing a union model for the center line and complete vessel information usage. We extracted the centerline with a new feature called degree of center field, which could be generated at the same time as vessel segmentation and avoid the deformation of bifurcation of vessels.

Plaque classification is challenging because of the need for an accurate segmentation algorithm, which may take thousands of data points and an understanding of vessel morphologic conditions. Several studies have developed AI models to simplify plaque characterization (30,31). For example, Matsumoto et al (32) investigated an automated function for evaluating low-attenuation plaque by excluding voxels adjacent to the outer vessel wall of arteries. The results showed an improvement in discriminating lipid-rich components. However, the arterial brain vessels were small, branched, and easily affected by extravascular tissues, which made it difficult for the algorithm to perform plaque detection and segmentation. Three-dimensional ResU-Net was performed to segment and detect plaques with the original axial image of head and neck CT angiography in our model. Moreover, we used a multifeature sequence callback model to reduce the false-positive rate caused by peripheral tissues and report the final classification results.

In addition, several studies have demonstrated that DL methods could allow quantitative measurements of coronary arterial stenosis and have high correlation with expert readers (16,32–34). In our study, the correlation between the AI model and experts was high. Also, several AI models have been developed to classify plaque characterization. However, most of these studies focus on coronary plaque, and few of them are used clinically. Zreik et al (35) used a multitask recurrent convolutional neural network to identify plaque characteristics (noncalcified, mixed, and calcified) at the vessel level with a weighted κ of 0.66. In comparison, our algorithm achieved a higher κ value of 0.78 because we used a multifeature sequence callback model that could achieve an accurate classification and reduce the false-positive rate.

Our study had several limitations. First, the clinical samples were relatively small, and the selection of patients was biased. Second, fatty component was not included in the

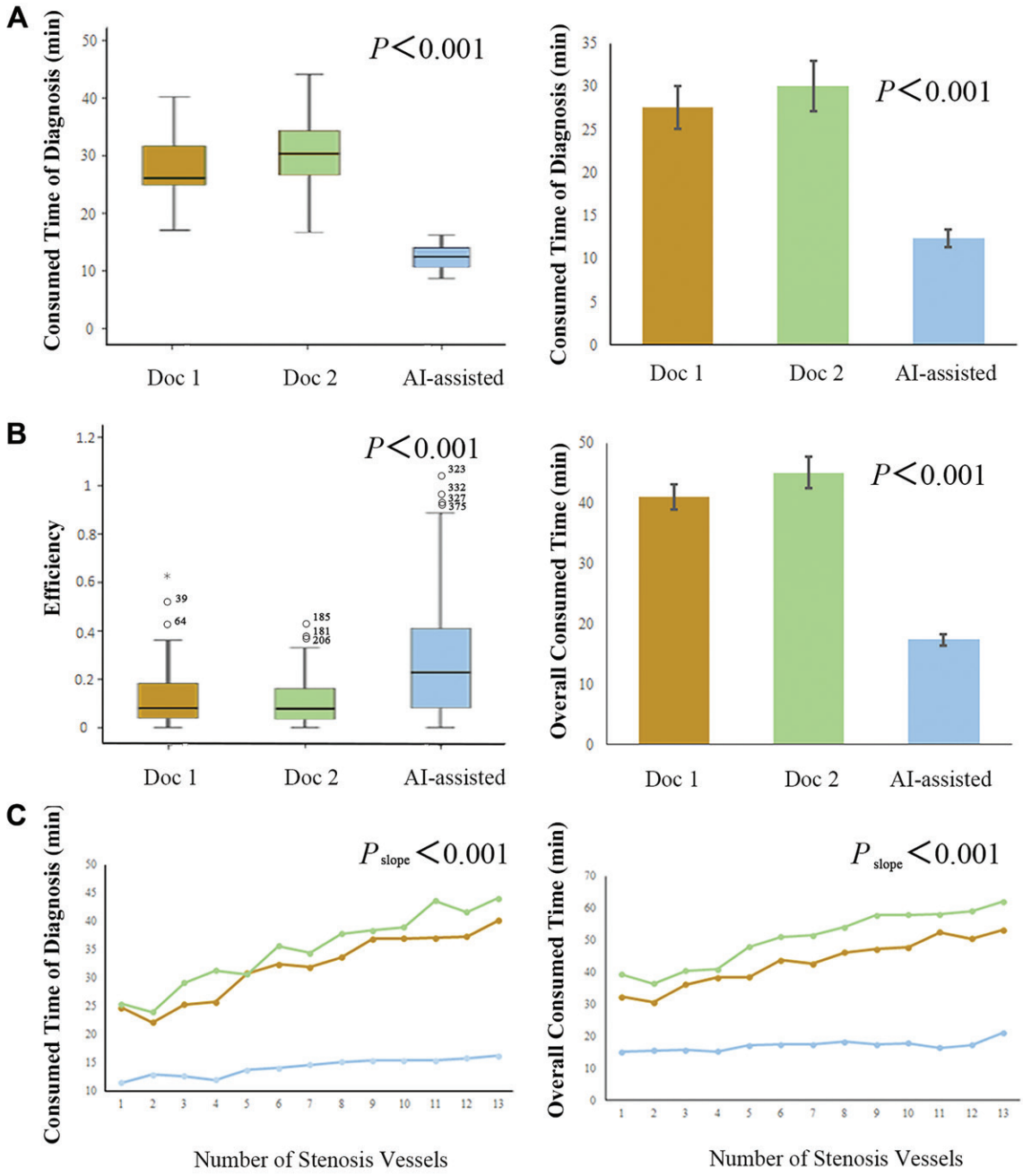

Figure 5: Charts show the comparison between the traditional head and neck CT angiography scans and deep learning–assisted algorithm. **(A)** Box and whisker plots show the average diagnostic consumed time between two radiologists and artificial intelligence (AI). **(B)** Box and whisker plots show the efficiency of the two radiologists improved when assisted by AI (efficiency was defined as the detected numbers of stenosis per unit time) and the overall time (including reconstruction, diagnosing, and reporting time) with and without AI. Boundaries of boxes indicate upper and lower quartiles and lines in boxes indicate medians. **(C)** Line charts show a significant difference between AI and radiologist for diagnosing reporting time ($F = 48.6$, $P < .001$) and overall time ($F = 59.3$, $P < .001$) with the increase of diseased vessels. P_{slope} means the significance test of slope in linear regression among three curves.

categorization of plaques because of the limitations of image resolution and the lack of accurate labeling. Third, the ground truth was the consensus of experienced radiologists without validation of the digital subtraction angiography.

In conclusion, in this pilot study, an automated convolutional neural network–based deep learning algorithm for head and neck CT angiography interpretation accurately determined vessel stenosis and plaque classification. The algorithm had equivalent diagnostic performance when compared with experienced radiologists. This algorithm offers a time-saving and accurate method to reconstruct, detect, classify, and lay out images of head and neck CT angiography to provide optimized clinical workflow. Multicenter and multivendor studies should be performed to evaluate the diagnostic robustness of our algorithm. Also, further validation is necessary with invasive digital subtraction angiography as the reference standard. Ongoing studies will

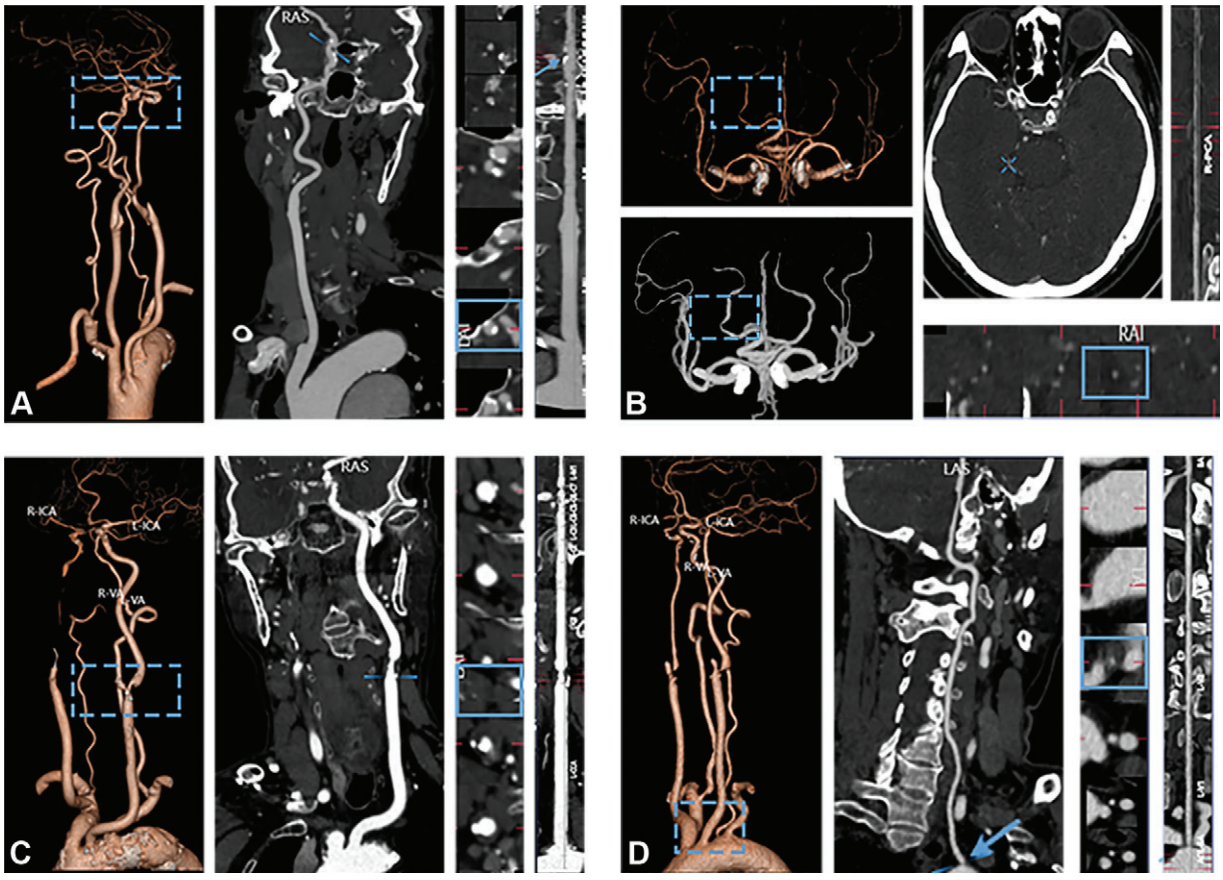

Figure 6: Muliple planners reformat, curve planner reformat, maximum intensity projection, and rendering images show the direct presentation of cases in threshold diagnosis. **(A)** The right internal carotid artery (ICA) was calculated with 51% stenosis of artificial intelligence (AI), and the radiologist's description was "mild to moderate" (arrow and boxes). **(B)** The right posterior cerebral artery was calculated with 47% stenosis of AI, and the radiologist's description was "moderate" (boxes). **(C)** The left internal carotid artery was calculated with 68% stenosis of AI, and the radiologist's description was "severe" (boxes). **(D)** The left vertebral artery (VA) was calculated with 78% stenosis of AI, and the radiologist's description was "moderate to severe" (arrow and boxes). LAS = left anterior superior, RAS = right anterior superior.

include patients with severe stenosis with use of invasive angiography as a reference.

Acknowledgments: We appreciate Suning Li, MD (Medical Statistician, YuKun [Beijing] Technology), for his kind assistance in statistical analysis and Duanduan Chen, MD, PhD (Biomechanics, School of Life Science, University of Beijing Institute of Technology), for her kind assistance in revising the manuscript.

Author contributions: Guarantors of integrity of entire study, **F.F., C.Z., M.Z., J.L.**; study concepts/study design or data acquisition or data analysis/interpretation, all authors; manuscript drafting or manuscript revision for important intellectual content, all authors; approval of final version of submitted manuscript, all authors; agrees to ensure any questions related to the work are appropriately resolved, all authors; literature research, **F.F., Y.S., C.Z., M.Z., J.L.**; clinical studies, **F.F., Y.S., C.Z., M.Z., X.W., J.L.**; experimental studies, **F.F., G.Y., C.Z., M.Z., D.R., J.L.**; statistical analysis, **F.F., C.Z., M.Z.**; and manuscript editing, **F.F., C.Z., M.Z.**

Disclosures of conflicts of interest: **F.F.** No relevant relationships. **Y.S.** No relevant relationships. **G.Y.** No relevant relationships. **C.Z.** No relevant relationships. **M.Z.** No relevant relationships. **D.R.** No relevant relationships. **X.W.** No relevant relationships. **J.L.** No relevant relationships.

References

1. Wu S, Wu B, Liu M, et al. Stroke in China: advances and challenges in epidemiology, prevention, and management. Lancet Neurol 2019;18(4):394–405.
2. Libby P. The changing landscape of atherosclerosis. Nature 2021;592 (7855):524–533.
3. Cademartiri F, Balestrieri A, Cau R, et al. Insight from imaging on plaque vulnerability: similarities and differences between coronary and carotid arteries-implications for systemic therapies. Cardiovasc Diagn Ther 2020;10(4):1150–1162.
4. Saxena A, Ng EYK, Lim ST. Imaging modalities to diagnose carotid artery stenosis: progress and prospect. Biomed Eng Online 2019;18(1):66.
5. Hilkewich MW. Written observations as a part of computed tomography angiography post processing by medical radiation technologists: A pilot project. J Med Imaging Radiat Sci 2014;45(1):31–36.e1.
6. Meijboom WB, Meijs MF, Schuijf JD, et al. Diagnostic accuracy of 64-slice computed tomography coronary angiography: a prospective, multicenter, multivendor study. J Am Coll Cardiol 2008;52(25):2135–2144.
7. Budoff MJ, Dowe D, Jollis JG, et al. Diagnostic performance of 64-multidetector row coronary computed tomographic angiography for evaluation of coronary artery stenosis in individuals without known coronary artery disease: results from the prospective multicenter ACCURACY (Assessment by Coronary Computed Tomographic Angiography of Individuals Undergoing Invasive Coronary Angiography) trial. J Am Coll Cardiol 2008;52(21):1724–1732.
8. Saba L, Biswas M, Kuppili V, et al. The present and future of deep learning in radiology. Eur J Radiol 2019;114:14–24.
9. Erickson BJ, Korfiatis P, Akkus Z, Kline TL. Machine learning for medical imaging. RadioGraphics 2017;37(2):505–515.
10. Chung M, Calabrese E, Mongan J, et al. Deep learning to simulate contrast-enhanced breast MRI of invasive breast cancer. Radiology 2022213199.
11. Mu D, Bai J, Chen W, et al. Calcium scoring at coronary CT angiography using deep learning. Radiology 2022;302(2):309–316.
12. Yang J, Xie M, Hu C, et al. Deep learning for detecting cerebral aneurysms with CT angiography. Radiology 2021;298(1):155–163.
13. Chilamkurthy S, Ghosh R, Tanamala S, et al. Deep learning algorithms for detection of critical findings in head CT scans: a retrospective study. Lancet 2018;392(10162):2388–2396.

14. Sim Y, Chung MJ, Kotter E, et al. Deep convolutional neural network-based software improves radiologist detection of malignant lung nodules on chest radiographs. Radiology 2020;294(1):199–209.
15. Titano JJ, Badgeley M, Schefflein J, et al. Automated deep-neural-network surveillance of cranial images for acute neurologic events. Nat Med 2018;24(9):1337–1341.
16. Hong Y, Commandeur F, Cadet S, et al. Deep learning-based stenosis quantification from coronary CT angiography. Proc SPIE Int Soc Opt Eng 2019; 10949. Conference:imaging Processing.
17. Candemir S, White RD, Demirer M, et al. Automated coronary artery atherosclerosis detection and weakly supervised localization on coronary CT angiography with a deep 3-dimensional convolutional neural network. Comput Med Imaging Graph 2020;83:101721.
18. Choi AD, Marques H, Kumar V, et al. CT evaluation by artificial intelligence for atherosclerosis, stenosis and vascular morphology (clarify): A multi-center, international study. J Cardiovasc Comput Tomogr 2021;15(6):470–476.
19. Dilsizian SE, Siegel EL. Artificial intelligence in medicine and cardiac imaging: harnessing big data and advanced computing to provide personalized medical diagnosis and treatment. Curr Cardiol Rep 2014;16(1):441.
20. Han D, Liu J, Sun Z, Cui Y, He Y, Yang Z. Deep learning analysis in coronary computed tomographic angiography imaging for the assessment of patients with coronary artery stenosis. Comput Methods Programs Biomed 2020;196:105651.
21. Coenen A, Kim YH, Kruk M, et al. Diagnostic accuracy of a machine-learning approach to coronary computed tomographic angiography-based fractional flow reserve: Result from the machine consortium. Circ Cardiovasc Imaging 2018;11(6):e007217.
22. Meshram NH, Mitchell CC, Wilbrand S, Dempsey RJ, Varghese T. Deep learning for carotid plaque segmentation using a dilated U-net architecture. Ultrason Imaging 2020;42(4-5):221–230.
23. Cheng J, Chen Y, Yu Y, Chiu B. Carotid plaque segmentation from three-dimensional ultrasound images by direct three-dimensional sparse field level-set optimization. Comput Biol Med 2018;94:27–40.
24. Yushkevich PA, Piven J, Hazlett HC, et al. User-guided 3D active contour segmentation of anatomical structures: significantly improved efficiency and reliability. Neuroimage 2006;31(3):1116–1128.
25. Kimmel R, Shaked D, Kiryati N, Bruckstein AM. Skeletonization via distance maps and level sets. Comput Vis Image Underst 1995;62(3):382–391.
26. Fu F, Wei J, Zhang M, et al. Rapid vessel segmentation and reconstruction of head and neck angiograms using 3D convolutional neural network. Nat Commun 2020;11(1):4829.
27. Livne M, Rieger J, Aydin OU, et al. A U-net deep learning framework for high performance vessel segmentation in patients with cerebrovascular disease. Front Neurosci 2019;13:97.
28. Lee JG, Jun S, Cho YW, et al. Deep learning in medical imaging: General overview. Korean J Radiol 2017;18(4):570–584.
29. Saba L, Sanfilippo R, Montisci R, Calleo G, Mallarini G. Carotid artery stenosis quantification: concordance analysis between radiologist and semi-automatic computer software by using Multi-Detector-Row CT angiography. Eur J Radiol 2011;79(1):80–84.
30. He Y, Yang G, Yang J, et al. Dense biased networks with deep priori anatomy and hard region adaptation: Semi-supervised learning for fine renal artery segmentation. Med Image Anal 2020;63:101722.
31. Han X, Luo N, Xu L, et al. Artificial intelligence stenosis diagnosis in coronary CTA: effect on the performance and consistency of readers with less cardiovascular experience. BMC Med Imaging 2022;22(1):28.
32. Matsumoto H, Watanabe S, Kyo E, et al. Improved evaluation of lipid-rich plaque at coronary CT angiography: head-to-head comparison with intravascular US. Radiol Cardiothorac Imaging 2019;1(5):e190069.
33. Chen M, Wang X, Hao G, et al. Diagnostic performance of deep learning-based vascular extraction and stenosis detection technique for coronary artery disease. Br J Radiol 2020;93(1113):20191028.
34. Liu CY, Tang CX, Zhang XL, et al. Deep learning powered coronary CT angiography for detecting obstructive coronary artery disease: The effect of reader experience, calcification and image quality. Eur J Radiol 2021;142:109835.
35. Zreik M, van Hamersvelt RW, Wolterink JM, Leiner T, Viergever MA, Isgum I. A recurrent CNN for automatic detection and classification of coronary artery plaque and stenosis in coronary CT angiography. IEEE Trans Med Imaging 2019;38(7):1588–1598.